Journal of Catalysis 285 (2012) 124–133

Contents lists available at SciVerse ScienceDirect

Journal of Catalysis

journal homepage: www.elsevier.com/locate/jcat

Tuning the selectivity for ring-opening reactions of methylcyclopentane over Pt catalysts: A mechanistic study from first-principles calculations

Zhi-Jian Zhao, Lyudmila V. Moskaleva [1], Notker Rösch *

Technische Universität München, Department Chemie and Catalysis Research Center, 85747 Garching, Germany

ARTICLE INFO

Article history:
Received 18 June 2011
Revised 9 September 2011
Accepted 20 September 2011
Available online 25 November 2011

Keywords:
DFT calculations
Pt(111)
Pt(211)
Methylcyclopentane
Ring-opening
Selectivity
Hydrogenolysis
Reaction mechanism

ABSTRACT

Using density functional calculations, we studied the conversion of methylcyclopentane to its ring-opening products: branched hexanes [2-methylpentane (2MP), 3-methylpentane (3MP)], as well as unbranched *n*-hexane (*n*Hx). We employed flat Pt(111) and stepped Pt(211) to describe terrace-rich large and defect-rich small Pt particles, respectively. On Pt(111), the barriers of all elementary steps for the paths leading to branched hexanes lie below 90 kJ mol^{-1}, while the formation of *n*Hx features a barrier of 116 kJ mol^{-1} in its C–C bond scission step. This higher barrier impedes the formation of *n*Hx on Pt(111) and thus rationalizes the experimental observations that terrace-rich large Pt particles selectively produce branched hexanes. However, on Pt(211), the barrier of C–C scission for the formation of *n*Hx decreases to 94 kJ mol^{-1}, thus implying enhanced formation of *n*Hx over the defects, in agreement with the essentially statistical product distribution observed with defect-rich small Pt particles.

1. Introduction

Currently, there is a strong interest in reducing air pollutants emitted during diesel combustion. These pollutants, such as nitrogen oxides, sulfur oxides, and particulate matter, are likely to have harmful effects not only on human health but also on the environment as a whole. Therefore, it is expected that stricter requirements will be imposed on diesel fuels regarding their content of sulfur and polynuclear aromatics as well as cetane number (CN) [1].

The CN of diesel fuels can be improved with the help of modern upgrading technologies, such as aromatics saturation and hydrocracking [2,3]. With the help of hydrodearomatization catalysts, the aromatics are hydrogenated to saturated cyclic components (naphthenes). Yet, even when most aromatics are saturated, the CN increase is limited by the composition of the initial feedstock. By comparison, hydrocracking improves the fuel quality by saturating aromatic rings and cracking the saturated naphthenic rings as well as branched alkanes to lighter products. The main problem of hydrocracking is that it is not easily controlled; extensive overcracking of the raw materials generates a large amount of lower-weight products which cannot be used as diesel fuel. To yield a notably higher CN, ideally, naphthenes should be converted to more paraffinic compounds with a low degree of branching while preserving the initial molecular weights. Therefore, finding approaches to selectively open naphthene rings with minimum cleavage of side chains is much desired for generating products that meet (or exceed) the ever-tightening environmental regulations.

Selective ring-opening (SRO) of naphthenes generally requires a bifunctional catalyst [4]: (i) highly dispersed noble metal particles, e.g., of Pt, Pd, Ir, Ru, or Rh, for hydrogenation or dehydrogenation, and (ii) an acidic support for cracking or isomerization. It is important to note that five-member hydrocarbon rings open much easier on metals than six-member rings [4–8]. Therefore, initial contraction of a six-member ring to a five-member ring, promoted by an acidic function of the support of the metal, facilitates and accelerates the overall hydrogenolysis process [9,10]. Subsequently, isomerized C5 products can move through the gas phase to an active site on a metal component and there undergo a ring-opening reaction, the selectivity of which depends on the nature of the metal.

As a model SRO reaction, ring-opening of methylcyclopentane (MCP) on supported metal catalysts has extensively been studied [11–16], for work until 2005, see an earlier review [4]. The distribution of the products, 2-methylpentane (2MP), 3-methylpentane (3MP), and *n*-hexane (*n*Hx), depends on the properties of the metal catalyst. For example, over supported Pt catalysts, such a distribution sensitively depends on the size of the Pt particles. A

* Corresponding author.
E-mail address: roesch@mytum.de (N. Rösch).
[1] Present address: Institut für Angewandte und Physikalische Chemie, Universität Bremen, 28359 Bremen, Germany.

0021-9517/$ - see front matter © 2011 Elsevier Inc. All rights reserved.
doi:10.1016/j.jcat.2011.09.021

non-selective distribution (statistical scission of endocyclic C–C bonds) is found on highly dispersed small Pt particles [17], whereas branched products, 2MP and 3MP, are favored on large Pt particles [18] or the flat Pt surfaces (1 1 1) and (1 0 0) [19,20]. In contrast, the selectivity on other noble metals, like Ir [12,21] and Rh [22], is less sensitive to the particle size. On both Ir and Rh, MCP hydrogenolysis always yields branched 2MP and 3MP, which are not the desired products with high CN. Other metal catalysts, e.g., Co [23] or Ru [24], lead to extensive hydrogenolysis, producing a significant amount of fragments. None of the above metal catalysts is selective toward *n*Hx, the preferred product, which features a larger CN than the branched isomers 2MP and 3MP. Recent studies on bimetallic catalysts, e.g., GePt [16] or RhPt [13], also did not show a promising selectivity toward *n*Hx.

Due to the complexity of the involved chemistry, the mechanism of SRO has not clearly been proved experimentally and thus far remained at a hypothetical level. On the other hand, computational studies based on methods of density functional theory (DFT) provide tools to gain a better understanding of elementary reaction steps of a complex reaction network [25–29]. The few theoretical studies concerned with the chemistry of MCP and its derivatives on metal surfaces mainly addressed the adsorption properties of five-member rings such as MCP [30], cyclopentane [31–33], and cyclopentene [32,34]. An early work [35] addressed at a semiempirical level the dehydrogenation of cyclopentene, but did not touch the ring-opening. In the present work, we explored the conversion of MCP to its ring-opening products on the flat Pt(1 1 1) and stepped Pt(2 1 1) surfaces. Our study shows how the selectivity is controlled by the surface geometry and rationalizes the experimentally observed particle size dependence of the selectivity on supported Pt catalysts.

2. Models and computational details

We carried out DFT slab model calculations with the plane-wave-based Vienna *ab initio* simulation package VASP [36,37]. We used the generalized gradient approximation in the form of the exchange–correlation functional PW91 [38]. The interaction between the atomic cores and electrons was described by the projector augmented wave (PAW) method [39,40]. In the structure optimizations, the Brillouin zone was sampled using a Monkhorst–Pack [41] mesh of $5 \times 5 \times 1$ k points with first-order Methfessel–Paxton smearing (smearing width of 0.15 eV) [42]. Subsequently, the energies were refined in a single-point fashion employing a $7 \times 7 \times 1$ k point grid. The valence wave functions were expanded in a plane-wave basis with a cutoff energy of 400 eV.

We represented the ideal Pt(1 1 1) and Pt(2 1 1) surfaces by periodic slab models of five layers each, repeated in a supercell geometry with at least 1-nm vacuum spacing between them. In the case of the stepped surface Pt(2 1 1), a slab comprises five layers of (1 1 1) orientation, but formally contains 15 layers perpendicular to the surface normal. The three "bottom" layers of each five-layer slab were kept fixed at the theoretical bulk-terminated geometry (Pt–Pt = 282 pm), and the remaining Pt atoms were allowed to relax during geometry optimizations, together with the adsorbates, until the force on each atom was less than 2×10^{-4} eV/pm. We used a (3×3) unit cell for Pt(1 1 1) and a (3×1) unit cell for Pt(2 1 1), both of them corresponding to surface coverage 1/9. We also located transition states at this coverage.

The binding energy (BE) of an adsorbate was determined from $BE = E_{ad} + E_{sub} - E_{ad/sub}$, where $E_{ad/sub}$ is the total energy of the slab model, covered with the adsorbate in the optimized geometry; E_{ad} and E_{sub} are the total energies of the adsorbate in the gas phase (ground state) and of the clean substrate, respectively. Calculations on gas-phase hydrocarbon species with open shells were carried out in a spin-polarized fashion. With the above definition, positive values of BE imply a release of energy or a favorable interaction.

Transition states (TSs) of the reactions were determined by applying the dimer method [43] or the nudged elastic band (NEB) method [44,45]. In the latter case, we used eight images of the system to form a discrete approximation of the path between fixed end points. The TS structures obtained in this way were further refined until the forces on atomic centers dropped below 2×10^{-4} eV/pm. We checked each optimized transition state structure with a normal mode analysis to ensure that only a single mode with an imaginary frequency exists.

3. Results and discussion

As stated in the introduction, MCP is mainly converted to the branched products 2MP and 3MP on the Pt(1 1 1) surface or on large Pt particles (e.g., of ~10 nm [46]). To rationalize this observation, Maire et al. [18] proposed a mechanism in which the C–C bond breaking of the five-member ring occurs via an ααββ-tetra-adsorbed intermediate (Fig. 1). Only a di-secondary CH_2–CH_2 cyclic bond can be dehydrogenated to form such an intermediate, to be cleaved subsequently. Due to the methyl substituent, the secondary–tertiary CH_2–CHMe bond can only form an ααβ-tri-adsorbed intermediate. Owing to the steric hindrance, edge-wise adsorption of the secondary–tertiary C–C bond and its hydrogenolysis are expected to be unlikely. The described mechanism involving dehydrogenative chemisorption prior to C–C bond breaking is supported by the loss of 3.5–5 hydrogen atoms on nickel and of 2–4 hydrogen atoms on platinum per molecule of propane when the system is in the temperature range where hydrocracking takes place [47]. DFT calculations [48,49] also support this idea showing that the barrier for C–C bond

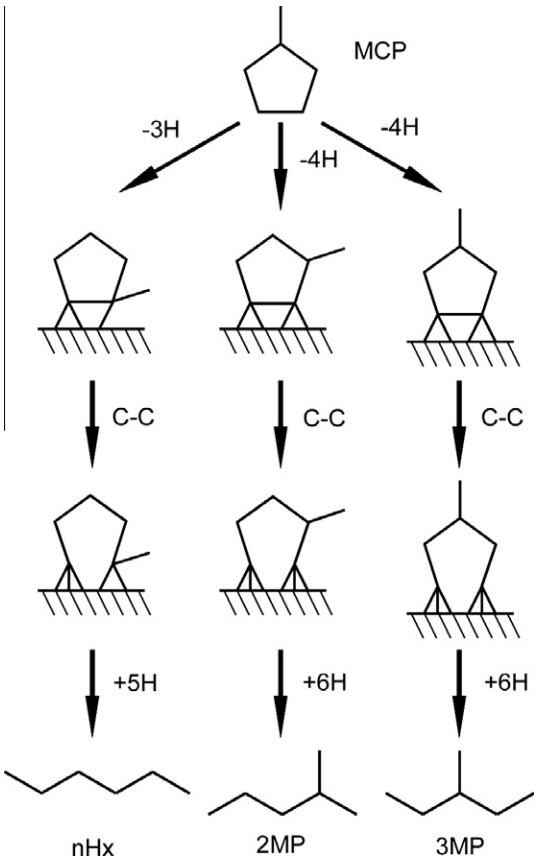

Fig. 1. The reaction network studied in this work.

cleavage of C_2 or C_3 species on M(1 1 1) (M = Pd, Pt) decreases with increasing the degree of dehydrogenation of the hydrocarbon.

Fig. 1 shows the reaction network investigated in this study. Building on the ideas of Maire et al. [18], we propose a mechanism with three global steps: (i) MCP is dehydrogenated to form an αααββ-tetra-adsorbed (or an ααβ-tri-adsorbed) intermediate; (ii) the C–C bond between the adsorbed C atoms is cleaved; (iii) the resulting adsorbate is completely hydrogenated and then desorbs from the surface. In the following discussion, we will address in turn these three sequential steps.

3.1. Dehydrogenation reactions over Pt(1 1 1)

To form an αααββ-tetra-adsorbed (or an ααβ-tri-adsorbed) intermediate, four or three dehydrogenation steps are required in the conversion from MCP to 2MP/3MP or *n*Hx, respectively. In each elementary step, one C–H bond of the ring structure is cleaved via a transition state that exhibits a typical C–H–Pt three-member-ring structure [50]. As an example, Fig. 2 illustrates the four dehydrogenation steps of the pathway to 3MP. Experimental studies [51] showed that the diffusion of H atoms on Pt requires very low activation energies of about 12 kJ mol^{-1}. Therefore, we refrained from studying the diffusion of H atoms between two dehydrogenation steps. We assume that the dissociating H atom moves far away from the adsorbate after each dehydrogenation step. Thus, in the surface unit cells of our models, there is at most one co-adsorbed H atom in each final (or initial, for hydrogenation reactions) state.

In the following, we will discuss the dehydrogenation reactions step by step. For each dehydrogenation reaction, the geometry of an adsorbate in the initial state is almost the same as in the final state of the preceding dehydrogenation step, except that in the final state, the dissociated H atom is still co-adsorbed on a surface close to the hydrocarbon, whereas in the initial state of the next dehydrogenation step it is no longer present in the model. Therefore, from the second dehydrogenation step, we will skip describing the structure of the initial state of a dehydrogenation reaction. When referring to the position of the methyl group within the ring, we shall denote, for convenience, the first C atom which binds to the metal surface as C1, and the second as C2; the other three carbon centers are numbered from C3 to C5 along the direction from C1 to C2.

3.1.1. First dehydrogenation reaction (D1)

We considered three adsorption modes of MCP corresponding to the three possibilities for the first dehydrogenation step according to the position of the methyl group which is attached to either of C1, C2 (C5), or C3 (C4). These three pathways have nearly identical geometries of the initial state; MCP is weakly adsorbed via an H atom attached to C1 so that a linear fragment Pt–H–C1 is formed in the direction normal to the surface (Fig. 2), with H–Pt = 210–211 pm. This weak H–Pt interaction also leads to an elongation of the corresponding C–H bond, to 114 pm, compared to 110 pm for the other C–H bonds. The binding energies of the three physisorbed intermediates are very similar, 14–16 kJ mol^{-1}. It should be noted that the GGA functional used is not able to describe such weak interactions in a quantitative way [52].

The three transition states of the first dehydrogenation step differ only by the position of the methyl substituent. In these transition states (see Fig. 2 for an example), the adsorbate tilts toward the surface so that the C1 atom arrives at the top site originally occupied by the dissociating H atom, while the leaving H atom is pushed to a bridge site of Pt(1 1 1). Due to the steric hindrance, the dissociating C–H bond of the transition state stretches significantly, to 161 pm, when CH_3 is attached at the C1 position. This distance is 13 pm longer than in the cases where the CH_3 group is at the C2 or C3 positions. This steric hindrance also leads

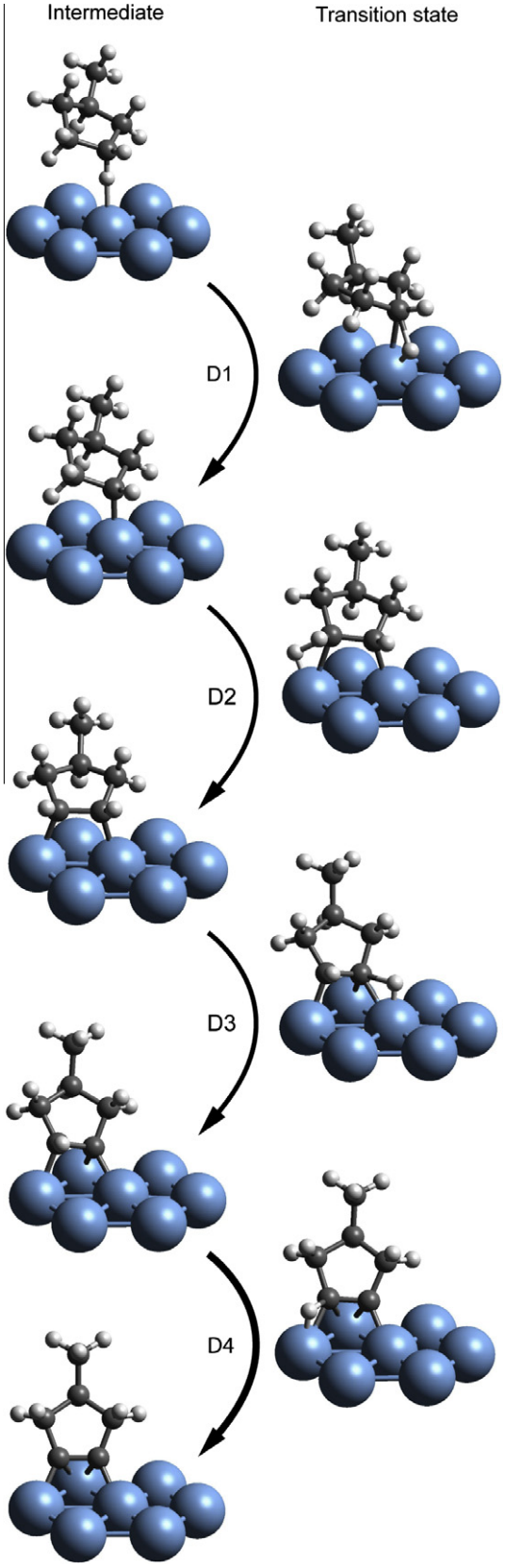

Fig. 2. Optimized structures corresponding to the four dehydrogenation steps (D1–D4) of the reaction path to 3MP. The intermediate and TS structures involved in the corresponding dehydrogenation steps on the way to 2MP and *n*Hx (not shown) are quite similar to these structures, only the position of the methyl group is changed.

to a slight increase in the total energy of the transition state structure, by ~11 kJ mol^{-1} with respect to the most stable TS structure where the CH_3 substituent is at the C3 position (Fig. S1).

In the final state (Fig. 2), the C–H bond totally breaks and the hydrocarbon is chemically adsorbed at a top site via a single C–Pt bond. When the methyl group is located at the C1 position, the steric hindrance not only elongates the C1–Pt bond length to 219 pm compared to the value of 212–213 pm when CH_3 is at the C2 or C3 positions, but also strongly pulls the Pt atom out of the surface, by ~50 pm. This latter value is twice as large as in the final states with the CH_3 group at the C2 or C3 position.

The activation energies of these three dehydrogenation reactions are rather similar: 97, 89, and 85 kJ mol^{-1} (Fig. S1), when the methyl group is bonded to the centers C1, C2, or C3, respectively. When the methyl group is bonded to C1, the barrier is 8–12 kJ mol^{-1} higher due to the steric hindrance just mentioned. However, the difference between the reaction energies is larger. In the sterically hindered case, the dehydrogenation is endothermic by ~36 kJ mol^{-1}, whereas the two alternative reactions are essentially thermoneutral (Fig. S1).

3.1.2. Second dehydrogenation reaction (D2)

There are several possible pathways to form the αααββ-tetra-adsorbed or ααβ-tri-adsorbed intermediates from MCP. Our calculation shows that the dehydrogenation barriers are similar (within 10 kJ mol^{-1}, Table 1) irrespective of whether the methyl group is connected to the centers C2, C3, C4, or C5. Therefore, we chose the pathways with the lowest barrier in the first dehydrogenation step; these are the routes starting with the CH_3 substituent at the C3 position (or at C4) on the way to 2MP (3MP) or at the C2 position on the way to *n*Hx, with the barriers of 85–89 kJ mol^{-1} for the first step (Table 1). Furthermore, for a selected initial state, at least two dehydrogenation reactions, α-elimination or β-elimination, compete with each other. Thus, two final states are possible, αα-diadsorbed or αβ-diadsorbed intermediates. Experimental evidence [53] suggests that in general β-H elimination reactions of a hydrocarbon fragment on Pt(1 1 1) are preferred over α-elimination reactions. These observations were corroborated by theoretical studies on Pt(1 1 1) [50] and Pd(1 1 1) [54] surfaces, which determined (at 1/9 coverage) barriers for β-elimination to be 10–25 kJ mol^{-1} lower than for α -elimination. Hence, in this step, we considered only the pathways involving β-H elimination to form αβ-diadsorbed intermediates.

In the initial states, the dehydrogenated MCP ring is adsorbed at a top site as described in the previous section. In the transition states (Fig. 2), center C2 is already attached to the surface and the dissociated H atom moves to a top site. Steric hindrance again is at work when CH_3 binds to C2. This is reflected not only in a longer C–Pt distance, by 14 pm, of the bond to be formed but also in a higher energy (by 8–15 kJ mol^{-1}) compared to the TS structures with the CH_3 substituent at C3 or C4 position. In the final states of this reaction, the dissociated H atom moves to the neighboring threefold hollow site. The adsorbate is adsorbed in μ–η^2 fashion via two σ bonds at a bridge site. All three reactions considered for this step are exothermic, by 17–31 kJ mol^{-1} (Table 1). The reaction barriers of the second dehydrogenation step fall into the range of 55–65 kJ mol^{-1}; thus, they are 24–30 kJ mol^{-1} lower than the barriers calculated for the first step D1 (Table 1).

3.1.3. Third dehydrogenation reaction (D3)

There are two choices for the loss of the third H atom in the reaction paths to 2MP or *n*Hx: either from C1 or C2. As shown above, the position of the methyl group does not significantly affect the activation energy; therefore, we chose to remove the third H atom from center C1 in all the three paths considered for step D3. In the transition state (Fig. 2), the carbon atom involved forms a second bond to a Pt center in bridging fashion, while the dissociating H atom interacts with both centers, Pt (162 pm) and C (155–156 pm) (Table 1). In the final state (Fig. 2), the H atom moves to a neighboring hollow site. The ααβ-dehydrogenated hydrocarbon adsorbate remains attached to the surface in μ_3–η^2 fashion as in the transition state. This reaction step is endothermic, by 21–26 kJ mol^{-1}; the corresponding activation energies are 84–88 kJ mol^{-1} (Table 1). In view of the relatively high calculated barrier for step D3, we checked the possibility of C–C bond cleavage in the αβ-dehydrogenated intermediate. Test calculations gave a higher estimate for the barrier, 148 kJ mol^{-1}. This value is significantly above the third dehydrogenation barrier and also much higher than the barriers for C–C bond activation of tri- and tetra-dehydrogenated intermediates (see below).

3.1.4. Fourth dehydrogenation reaction (D4)

After the three dehydrogenation steps, the intermediates are attached to the surface by two adjacent carbon centers, C1 and C2, of

Table 1
Optimized geometries[a] (pm) and energy characteristics (kJ mol^{-1}) of the transition states pertinent to the MCP ring-opening reactions over Pt(1 1 1) for various locations of the methyl (Me) substituent.

Reaction step[b]	2MP as product (Me at C3)				3MP as product (Me at C4)				*n*Hx as product (Me at C2)			
	C–H[c]	H–Pt[c]	ΔE[d]	E_a[e]	C–H[c]	H–Pt[c]	ΔE[d]	E_a[e]	C–H[c]	H–Pt[c]	ΔE[d]	E_a[e]
D1	148	167, 214	0	85	148	167, 214	0	85	148	167, 213	0	89
D2	157	160	−31	55	155	160	−30	57	165	159	−17	65
D3	155	162	21	84	155	162	24	88	156	162	26	86
D4[f]	144	163	−18	60	144	163	−20	58				
Migration[f]			60	61			60	61				
CC			−21	15			−21	14			−19	116
C-shift1[f]			−71	14			−73	15				
C-shift2[f]			−12	50			−10	52				
H1[f]	144	164	66	80	142	165	55	76				
H2	158	161	−4	56	155	161	−12	59	158	161	12	65
H3	156	170, 204	−43	66	150	168, 217	−24	72	161	175, 185	−57	52
H4[g]	136	166	78	83					135	167	78	81
H5[g]									157	162	−18	64
H6[g]									152	166, 221	−12	63

[a] A–B, distance between atoms A and B in the transition state.
[b] D1–D4 denote the first to fourth dehydrogenation steps; CC stands for the C–C bond scission step; H1–H6 refer to the first to sixth hydrogenation steps.
[c] Bonds that are breaking/forming during a reaction.
[d] Reaction energy.
[e] Activation energy.
[f] The reaction path to *n*Hx does not contain this step.
[g] The fourth to sixth hydrogenation steps for 2MP and 3MP are expected to have very close energy profile as the respective hydrogenation steps for *n*Hx.

the backbone of the ring. For the intermediates finally converting to 2MP or 3MP, one H atom is still to be removed from one of these two carbon centers. However, on the pathway to *n*Hx, the position of this H atom is occupied by the methyl substituent. Therefore, only the two pathways, leading to 2MP or 3MP as final products, are addressed in step D4. In the transition state (Fig. 2), C1 and C2 occupy two bridge positions of the same hollow site of Pt(1 1 1) with two C–Pt bonds per C atom. The C–C distance, only 142 pm, is shorter than in the initial state, 149 pm. The dissociated H atom migrates over a top site. The whole ring is oriented almost perpendicular to the Pt surface. The structure of the final state (Fig. 2) is very close to that of the transition state, except that the C–H bond is totally broken and the dissociated H atom has moved to a neighboring hollow site. This reaction is exothermic by 18–20 kJ mol^{-1}, and the barrier of this reaction is not very high, 58–60 kJ mol^{-1} (Table 1).

3.2. C–C bond breaking reactions over Pt(1 1 1)

Via the sequence of dehydrogenation reactions just described, we arrive at three intermediates: ααββ-tetra-adsorbed 3-methylcyclopentyne and 4-methylcyclopentyne as well as ααβ-tri-adsorbed 2-methyl-1-cyclopenten-1-yl. The former two intermediates ultimately convert to 2MP and 3MP, respectively, whereas the latter intermediate converts to *n*Hx. The C–C bond breaking reactions of the ααββ-tetra-adsorbed (tetra-dehydrogenated) intermediates and of the ααβ-tri-adsorbed (tri-dehydrogenated) intermediate represent two types of reactions each of which will now be discussed.

3.2.1. C–C bond breaking in the tetra-dehydrogenated intermediates

In the initial state (Fig. 3), the ring structure is almost normal to the surface and the C–C bond is located above a threefold hollow site so that one Pt atom forms bonds to both C atoms and the two other Pt atoms form one C–Pt bond each. Our attempt to find a TS for C–C bond breaking directly from this intermediate led to a second-order TS, 130 kJ mol^{-1} above the reactant, with the imaginary modes corresponding to C–C bond stretching and to a migration of the whole molecule in the direction of an adjacent threefold hollow site. Thus, the lowest energy pathway for C–C scission passes through an intermediate. Before the C–C bond is broken, the whole structure of the adsorbate rotates by ∼30° about the surface normal and is shifted in the direction of the C–C bond so that at the new location two C atoms occupy two adjacent threefold hollow sites (Fig. 3) with C–C = 148 pm. This change in adsorption site, which we further refer to as migration, is strongly endothermic by about 60 kJ mol^{-1} with a very low reverse reaction barrier, 1 kJ mol^{-1} (Table 1). It should be noted that multiple adsorption modes were also reported for acetylene adsorbed on transition metal surfaces [55].

After the migration step, the C–C bond breaks easily. In the transition state, the C–C distance is elongated by 28–30 pm, to 176–178 pm. In the final state, C–C = 237 pm. A surprisingly low barrier, only 14–15 kJ mol^{-1}, is calculated for this elementary step. The reaction is exothermic by 21 kJ mol^{-1} (Table 1). However, due to the extremely low reverse barrier (1 kJ mol^{-1}) for the preceding migration step, the total barrier should be calculated relative to the most stable configuration of the tetra-adsorbed cyclic species; it thus includes the energetic cost of the migration step, 60 kJ mol^{-1}. Therefore, the overall barrier to overcome the combined migration and C–C bond scission amounts to 74–75 kJ mol^{-1} (Table 2).

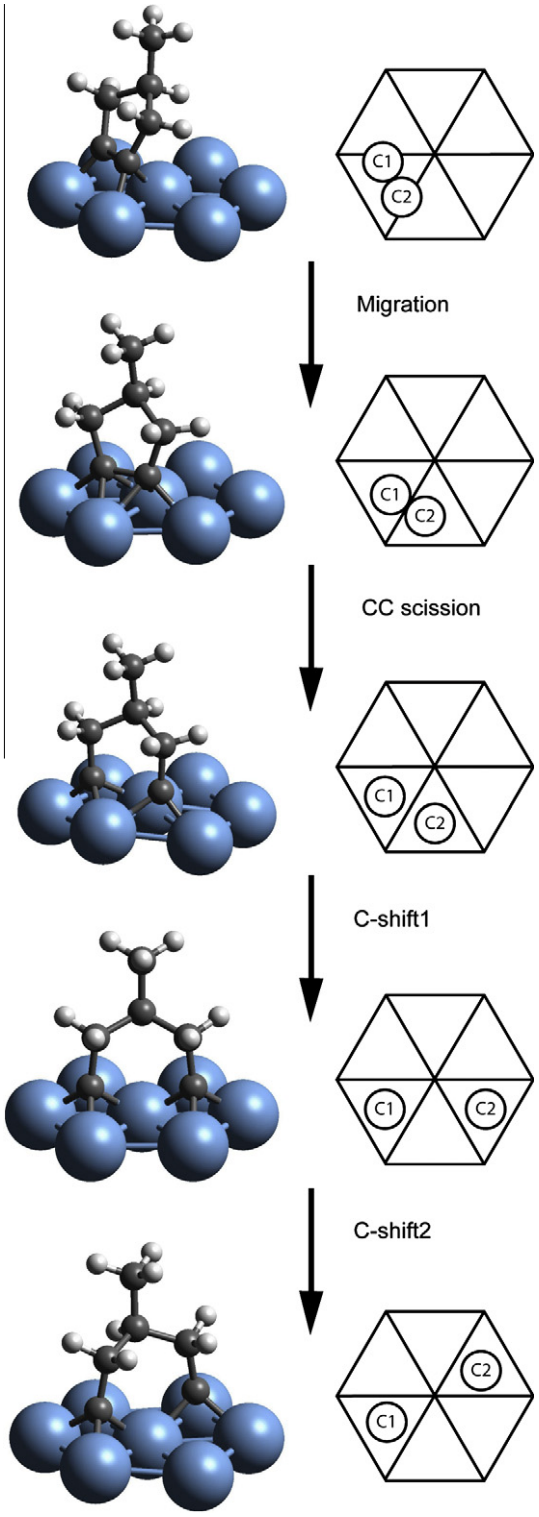

Fig. 3. Optimized initial and final structures and a schematic illustration of the adsorption modes for the migration, C–C bond scission, and C-shift steps on the way to 3MP. C1 and C2 denote the two C atoms which are directly bound to Pt(1 1 1). The intermediate structures of the corresponding steps involved in the pathways to 2MP (not shown) differ mainly by the position of the methyl group.

3.2.2. C–C bond breaking in the tri-dehydrogenated intermediate

In contrast to the tetra-dehydrogenated intermediate, the C–C bond breaking of the adsorbate attached to one threefold site in μ_3–η^2 fashion (Fig. 4) can proceed directly. In the initial state, the C–C distance is 150 pm. As shown in Fig. 4, in the transition state, the C atom to which the CH_3 group is attached migrates to a neighboring top site while the other adsorbed C center moves only slightly toward the center of a threefold site, whereby the C–C bond elongates to 212 pm. In the final state, the former C atom moves over a top site and attaches at a bridge site, while the latter

Table 2
Optimized geometries[a] (pm) and energy characteristics (kJ mol^{-1}) of the transition states for the C–C scission step in MCP ring-opening reactions over Pt(1 1 1) and Pt(2 1 1).

Surface	2MP as product			3MP as product			*n*Hx as product		
	C–C [b]	ΔE [c]	E_a [d]	C–C [b]	ΔE [c]	E_a [d]	C–C [b]	ΔE [c]	E_a [d]
Pt(1 1 1)	178	−21	75	176	−21	74	212	−19	116
Pt(2 1 1)	189	33	98	191	40	102	203	12	94

[a] A–B, distance between atoms A and B in the transition state.
[b] Bonds that are breaking/forming during a reaction.
[c] Reaction energy.
[d] Activation energy.

carbon center occupies the threefold hollow site which initially hosted both C atoms (Fig. 4). With C–C = 303 pm, the C–C bond is completely broken. This reaction is exothermic by 19 kJ mol^{-1} (Table 2). Unlike the tetra-dehydrogenated intermediate, the tri-dehydrogenated ring cleaves with a notably higher barrier, 116 kJ mol^{-1}. This barrier is at least 27 kJ mol^{-1} higher than the barriers of the preceding dehydrogenation reactions (Table 1).

3.3. Hydrogenation reactions over Pt(1 1 1)

The C6 species resulting from C–C scission has to undergo re-hydrogenation before the final product, 2MP, 3MP, or *n*Hx, is formed. Similar to the dehydrogenation reactions of MCP considered in Section 3.1, the order in which the H atoms can be added to the two unsaturated C centers is not unique. One has two major choices for this sequence of reactions: (i) first total hydrogenation of one terminal carbon center, followed by the total hydrogenation of the second carbon center, or (ii) alternating hydrogenation steps at the two terminal carbon centers. Our earlier theoretical study [50] on the transformations of C_2H_x (x = 2–5) species on Pt(1 1 1) showed that the activation energy of the hydrogenation of the carbyne species CCH_3, 89 kJ mol^{-1}, is 21 kJ mol^{-1} higher than the barrier for hydrogenating the carbene species $CHCH_3$. When hydrogenating a carbynic terminal C atom in the present work, we calculated here a similarly high barrier, 76–97 kJ mol^{-1}, whereas the activation energies are only 56–72 kJ mol^{-1} for the hydrogenation reactions of carbenic or monoradical carbon centers considered in this study. Furthermore, the hydrogenation of a carbynic C is strongly endothermic, by 55–78 kJ mol^{-1}; in line with that, the barrier for the reverse reaction is very low, only 5–21 kJ mol^{-1}, rendering this hydrogenation step slow. Therefore, in the energetically preferred hydrogenation variant, one of the two terminal C atoms is completely hydrogenated and detached from the surface before the hydrogenation of the other one starts due to the high activation energies for hydrogenating of the carbyne center (H1, H4). In the following, we will separately discuss the chains of hydrogenation reactions that lead to each of the final products. Figs. 5 and 6 show characteristic structures on the hydrogenation pathways to *n*Hx and 3MP, respectively.

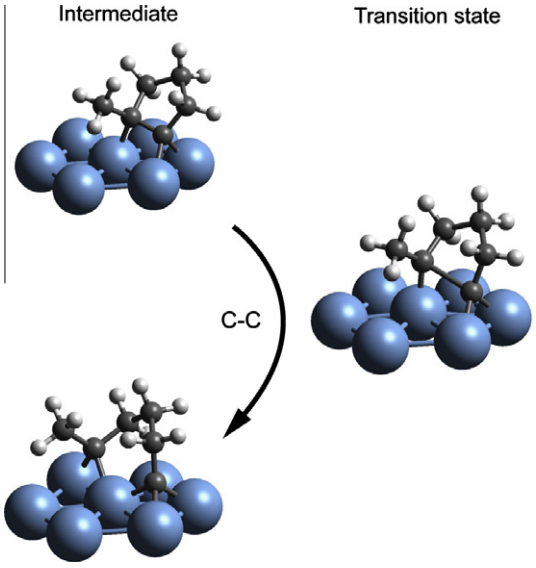

Fig. 4. Optimized structures for the C–C bond scission step on the reaction path to *n*Hx at Pt(1 1 1).

3.3.1 Pathways to form nHx (H2–H6)

The precursor of *n*Hx, formed after C–C bond cleavage, is 1-methylpentan-1-yliden-5-ylidyne. This species of carbene/carbyne type, briefly introduced in Section 3.2, is bound to four Pt atoms, three of which belong to a same threefold site. In the structure of this adsorption complex, one of the unsaturated C atoms occupies that hollow site while the other one (with a CH_3 substituent attached to it) binds in bridge mode to two Pt atoms (Fig. 5). As discussed above, the carbenic C atom is hydrogenated first, by two H atoms, to complete saturation (Fig. 5; reactions H2, H3). Subsequently, the carbynic C atom is hydrogenated to complete saturation (Fig. 5, reactions H4–H6). Finally, the alkane molecule desorbs from the surface. Energetically, nearly all hydrogenation reactions (H2, H3, H5, H6) on the pathway to *n*Hx are exothermic or slightly endothermic (12 kJ mol^{-1}) with activation energies of 52–65 kJ mol^{-1} (Table 1). The only exception is the first hydrogenation of the carbynic C atom (H4 in Fig. 5), which is strongly endothermic, by 78 kJ mol^{-1} (Table 1), with an extremely low backward barrier of only 3 kJ mol^{-1}. Similarly, low barriers had also been calculated in our earlier studies [50,56] on the hydrogenation of CCH_3, 19 kJ mol^{-1} over Pt(1 1 1) and 25 kJ mol^{-1} over Pd(1 1 1).

3.3.2. Pathways to form 2MP and 3MP

3.3.2.1. C-shift reactions (C-shift1, C-shift2). After C–C bond breaking, the two products, 2-methylpentan-1,5-diylidyne and 3-methylpentan-1,5-diylidyne, are characterized by the same adsorption mode: two terminal C atoms are adsorbed at adjacent threefold hollow sites (Fig. 3). The CH_3 group is attached to the C3 or C4 atom of the intermediate on the reaction paths to 2MP or 3MP, respectively. This adsorption mode, however, is not energetically the most stable one. As Fig. 3 illustrates, a shift reaction (C-shift1) leads to a less strained configuration in which two carbynic C centers occupy threefold sites further apart. The corresponding energy gain is ~70 kJ mol^{-1}, and the barrier is very low, 15 kJ mol^{-1} (Table 1), i.e., much lower than the typical barrier of a hydrogenation reaction (~50–100 kJ mol^{-1}).

Now, the two terminal C atoms are adsorbed at two threefold hollow sites that are separated by another threefold hollow site (Fig. 3). The activation energy for a direct hydrogenation of the C-shift1 product was calculated rather high, 95–97 kJ mol^{-1} for both reaction paths to 2MP and 3MP. Therefore, another shift step for the adsorbed C atom is added, which moves one C atom to its

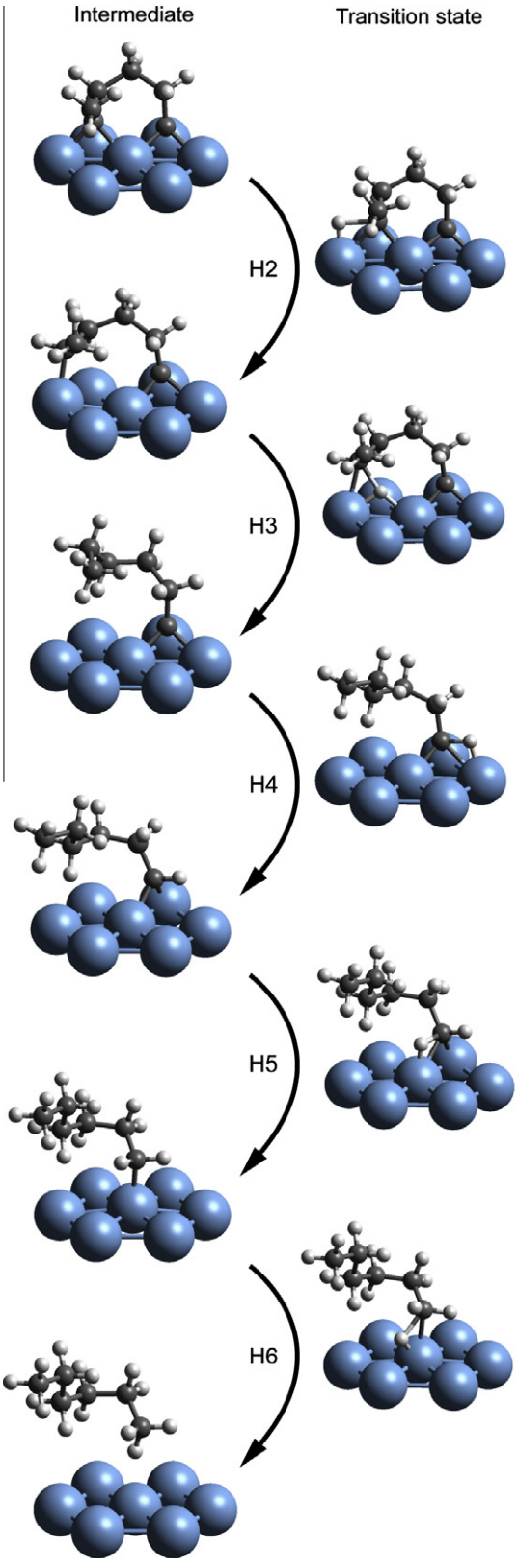

Fig. 5. Optimized structures corresponding to the second to sixth hydrogenation steps (H2–H6) on the reaction path to *n*Hx. The intermediate and TS structures of the corresponding hydrogenation steps involved in the pathways to 2MP and 3MP (not shown) differ mainly by the position of the methyl group.

neighbor threefold hollow site so that finally the two carbynic C atoms are positioned diametrically opposite to each other in a hexagon (Fig. 3). The second shift reaction is slightly exothermic,

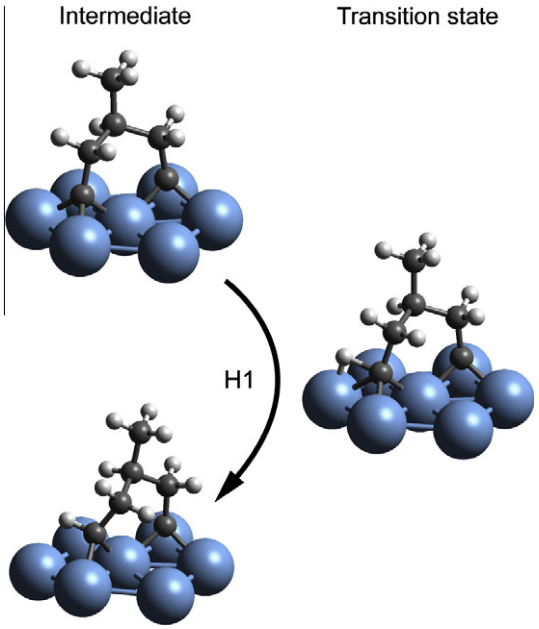

Fig. 6. Optimized structures for the first hydrogenation step (H1) on the reaction path to 3MP. The intermediate and TS structures of the corresponding hydrogenation steps involved in the pathways to 2MP (not shown) differ mainly by the position of the methyl group.

by 10–12 kJ mol^{-1}, with an activation energy of 50–52 kJ mol^{-1} (Table 1). After this additional rearrangement, the barrier of the next hydrogenation step was calculated notably lower than after C-shift1, 76–80 kJ mol^{-1} (Table 1). This finding can be rationalized by a less strained structure than that of the corresponding TS after the first C-shift; for a detailed discussion see Supplementary data.

3.3.2.2. Hydrogenation reactions to 2MP and 3MP (H1–H6). In total, there are six hydrogenation steps on the way to 2MP or 3MP. Fig. 6 shows the characteristic structures for step H1 on the pathway to 3MP. The structures for the subsequent hydrogenation steps H2–H6 are analogous to those shown for the pathway to *n*Hx (Fig. 5). In the case of the 2MP precursor, which is asymmetric, there are two possibilities for adding the first hydrogen. As the energetics of dehydrogenation/hydrogenation reactions is not sensitive to the position of the methyl group at C3–C5 (as shown above in our discussion on the dehydrogenation reactions), we chose the reaction path with the terminal C atom close to the methyl group to be hydrogenated first.

The hydrogenation of the carbynic C atom (reaction H1) is strongly endothermic, by more than 55 kJ mol^{-1}, with relatively low reverse barriers, 21–24 kJ mol^{-1} (Table 1). The other two reaction steps, H2 and H3, are exothermic, with reaction energies ranging from −4 kJ mol^{-1} to −43 kJ mol^{-1} and the activation energies of 56–72 kJ mol^{-1} (Table 1).

After the first three hydrogenation steps, 3-methylpentylidyne or 4-methylpentylidyne are adsorbed on the surface in the same way as the carbynic precursor of *n*Hx, hexylidyne, discussed in the preceding section. The total energies of the initial, transition, and final state for the hydrogenation of 4-methylpentylidyne are calculated only about 3–5 kJ mol^{-1} lower than the corresponding states in the hydrogenation step of hexylidyne. Therefore, we assume the three hydrogenation steps (H4–H6) to have the same barrier as the analogous hydrogenation steps of the path to *n*Hx.

3.4. C–C bond breaking reactions over Pt(211)

To check how surface defects may affect the selectivity, we also considered the ring-opening of MCP at the stepped surface

Pt(2 1 1), which is a model system with line defects. Experimental evidence suggests that the activity toward C–C bond scission increases at stepped or kinked Pt surfaces [57]. Focusing our computational effort, we refrained from exploring the pathways for the relevant hydrogenation and dehydrogenation reactions over the stepped surface; such reactions are considered insensitive to the surface structure [58]. Earlier computational studies on the decomposition of propane [49] and ethane [59] also showed that activation energies of dehydrogenation reactions analogous to those discussed in the present work over stepped surfaces Pt(2 1 1) and Pt(1 1 0) lie in range of 20–70 kJ mol^{-1}. Hence, we addressed only the C–C bond scission steps over the surface Pt(2 1 1).

This stepped surface offers more possibilities for adsorption sites and the relative orientation of the dehydrogenated C6 species undergoing C–C bond scission. Here, we only report on the pathways with relatively low activation energies for C–C bond scission; see Supplementary data for details of alternative reaction routes. The initial states, tri- or tetra-dehydrogenated intermediates, are characterized by the hydrocarbon adsorbed at a hollow site close to the edge (Fig. 7). The structures of the initial states of all three routes (to 2MP, 3MP, and *n*Hx) are very similar to those of the corresponding stationary points over the flat surface Pt(1 1 1). The transition state structure on the path to *n*Hx is very similar to the corresponding TS over the Pt(1 1 1) surface (Fig. 4), whereas the paths to 2MP/3MP proceed without a migration step, at variance to the reaction routes over flat Pt(1 1 1). This difference probably is due to the fact that Pt atoms at a terrace edge bind the adsorbate rather strongly and prevent its migration away from the edge. In the final state structures (Fig. 7), the terminal C atoms bonded at the terrace edge are sp^2 hybridized, manifesting an additional π interaction with the metal atoms at the step edge. This is reflected both by the planar geometry of the interacting C centers and shorter C–Pt bonds (less than 200 pm). Such a π interaction, which is not observed over Pt(1 1 1), results from free bonding capacities offered by undercoordinated Pt atoms at edges.

The activation energies change noticeably. The barrier of C–C bond cleavage in the tri-dehydrogenated precursor of *n*Hx decreases from 116 kJ mol^{-1} to 94 kJ mol^{-1}, whereas the barriers for the ring-opening of the tetra-dehydrogenated intermediates on the reaction paths to 2MP and 3MP even increase, from 74 kJ mol^{-1} to 102 kJ mol^{-1} (2MP) and from 75 kJ mol^{-1} to 98 kJ mol^{-1} (3MP). We also checked the possibility for ring-opening of tri-dehydrogenated intermediates on the reaction paths to 2MP and 3MP (i.e., analogous to the C–C bond cleavage in the tri-dehydrogenated precursor of *n*Hx discussed above, except that the methyl group is now attached to C3 or C4). The barriers were calculated slightly higher than for the ring-opening of the tetra-dehydrogenated intermediates, 113 kJ mol^{-1} (2MP) and 111 kJ mol^{-1} (3MP).

3.5. Particle size effects on the selectivity of the ring-opening of MCP

Experimental studies on the ring-opening of MCP over supported Pt catalysts clearly show that the selectivity is strongly affected by the size of the Pt particles. Large particles [18,46] or flat Pt single crystal surfaces [19,20] favor branched products, 2MP or 3MP. When the particle size becomes smaller (~2 nm) [46], a statistical distribution of the products is obtained [17]: 2MP:3MP:*n*Hx = 0.4:0.2:0.4. Thus, all five C–C bonds in the five-member ring have an equal chance to be broken. With our model results, one can suggest a rationalization of these observations. Note in particular that the calculated activation energy for C–C bond scission on the way to *n*Hx over the Pt(1 1 1) terraces, 116 kJ mol^{-1}, is quite a bit higher than the barriers for C–C scission in the precursors of 2MP and 3MP, 74–75 kJ mol^{-1}. In fact, that barrier for C–C cleavage over Pt(1 1 1) is rate determining on the path to *n*Hx because it is also higher than the activation energies of the

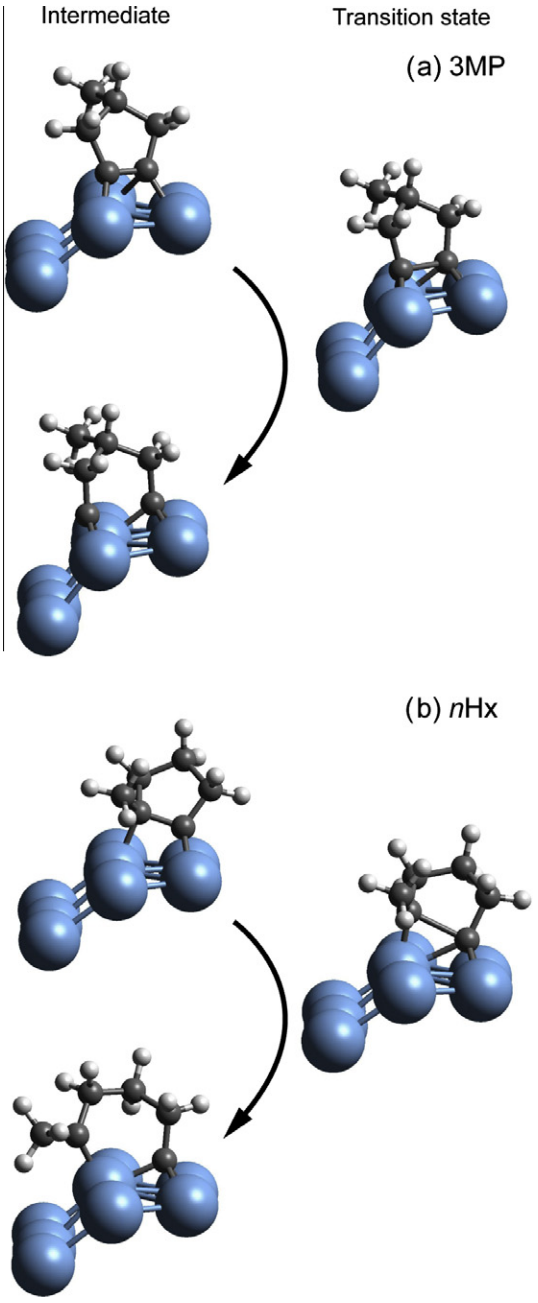

Fig. 7. Optimized structures of the C–C bond scission step over Pt(2 1 1): (a) on the reaction path to 3MP. The intermediate and TS structures of the corresponding steps of the path to 2MP (not shown) differ mainly by the position of the methyl group; (b) on the reaction path to *n*Hx.

hydrogenation and dehydrogenation reactions, which are less than 89 kJ mol^{-1} (Table 1, Fig. 8). In contrast, over steps, the barrier of C–C scission to form *n*Hx, calculated at 94 kJ mol^{-1}, is slightly lower than the barriers of C–C cleavage on the way to branched products, 102 kJ mol^{-1} (2MP) and 98 kJ mol^{-1} (3MP).

In this context, several relevant experiments deserve to be mentioned. Garin et al. [19] compared the selectivity of MCP ring-opening on the flat Pt(1 1 1) and the stepped Pt(5 5 7) surfaces. On Pt(1 1 1), the distribution of the products 2MP, 3MP, and *n*Hx was 0.6:0.3:0.1. Compared with the statistical ratio, 2MP:3MP:*n*Hx = 0.4:0.2:0.4, 2MP, and 3MP are clearly preferred. Over the stepped surface Pt(5 5 7), the relative yield of *n*Hx increased from 0.1 to 0.16, which nevertheless is much less than the statistically expected branching fraction 0.4. These results are not surprising

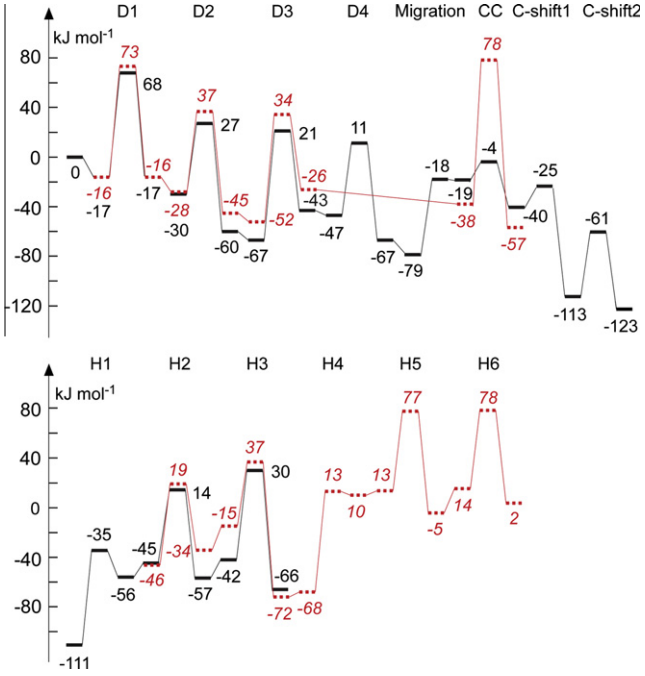

Fig. 8. The energy profiles (kJ mol^{-1}) of the MCP ring-opening reactions over Pt(1 1 1): reaction path to 3MP – solid (black) bars; reaction path to *n*Hx – dashed (red) bars. Energies are calculated relative to MCP(g) and the clean 3×3 Pt(1 1 1) slab. For a system containing x H atoms in the unit cell with energy E_{unitcell}, the relative energy is defined as $E = E_{\text{unitcell}} + (12 - x)\ (E_{\text{H/Pt(111)}} - E_{\text{Pt(111)}}) - E_{\text{MCP(g)}} - E_{\text{Pt(111)}}$. $E_{\text{H/Pt(111)}}$, $E_{\text{MCP(g)}}$, and $E_{\text{Pt(111)}}$ are the total energies of H adsorbed on Pt(1 1 1) at 1/9 coverage, of MCP (in the gas phase) and of the clean 3×3 Pt(1 1 1) slab, respectively. The energy shifts between two hydrogenation / dehydrogenation steps reflect the differences between a co-adsorbed H atom in the unit cell and an H atom at large distance (i.e., calculated separately on Pt(1 1 1) at 1/9 coverage). (For interpretation of the references to color in this figure legend, the reader is referred to the web version of this article.)

because (1 1 1) terraces encompass 86% of the Pt(5 5 7) surface atoms; thus, 2MP and 3MP are still preferentially produced over the terrace part of the stepped surface.

Zaera et al. [20] did not find an increase in the fraction of *n*Hx produced on the stepped Pt(5 5 7) surface. The difference to the observations of Garin et al. [19] may be rationalized by the lower H_2/MCP ratio used in the work of Zaera et al. [20]. Hence, under these latter experimental conditions, steps and other defects were blocked by carbonaceous deposits, as the authors confirmed by CO titration and Auger electron spectroscopy. Thus, carbon residues, which preferentially stick to undercoordinated surface sites [60,61], were found to inhibit the formation of *n*Hx over the steps.

In contrast, a statistical distribution of the branched products 2MP and 3MP as well as straight-chain *n*Hx is observed on small Pt particles [46]. One expects the difference to the results of large particles to be associated with the increased fraction of defect sites compared to regular terrace sites. The activation energies of C–C scission of all the three products (2MP, 3MP, and *n*Hx) are quite similar when the reaction occurs close to edge sites. Thus, the distribution of the products is expected to be closer to a statistical one when the particles are smaller and the ratio of edge sites to terraces sites increases.

4. Conclusions

We studied the conversion of methylcyclopetane (MCP) to its ring-opening products: 2MP, 3MP, and *n*Hx over the catalyst surfaces Pt(1 1 1) and Pt(2 1 1). In our model, the conversion entails three major steps: (i) dehydrogenation of MCP to an αααββ-tetra-adsorbed cyclic intermediate (as previously suggested by Maire et al. [18]) or an ααβ-tri-adsorbed cyclic intermediate, (ii) endocyclic C–C bond scission, and (iii) rehydrogenation. We calculated the transition state structures and activation energies for all these elementary steps on the Pt(1 1 1) surface and the activation energies for C–C bond cleavage on the stepped surface Pt(2 1 1).

The results of our calculations show that the activation energies of pertinent hydrogenation–dehydrogenation steps considered on the reaction paths to the various products over the Pt(1 1 1) surface fall in the range of 60–90 kJ mol^{-1}. However, the barrier for the C–C bond breaking step varies notably: from 74 kJ mol^{-1} to 116 kJ mol^{-1}.

These calculated results shed some light on the effect of particle size on the product distribution of ring-opening if we take the flat surface Pt(1 1 1) as a model of large Pt particles and the stepped surface Pt(2 1 1) as a model of edge sites on small Pt particles. Previous experimental studies noted that the branched products, 2MP and 3MP, were favored for large Pt particles or Pt single crystals. This observation is supported by the results of our calculations, which predict the activation energies of the C–C bond scission step on the pathways to 2MP and 3MP to be notably lower (at most 75 kJ mol^{-1}) than the barrier of C–C bond scission on the reaction path to *n*Hx, 116 kJ mol^{-1}. In fact, this latter barrier is ~27 kJ mol^{-1} higher than the barriers of all other elementary steps (dehydrogenation, hydrogenation), including the steps on the path to 2MP and 3MP. With such a higher rate-limiting barrier on the path to *n*Hx one is able to rationalize the lower yield of *n*Hx compared to 2MP and 3MP. However, this barrier of C–C cleavage on the way to *n*Hx drops to 94 kJ mol^{-1} on the Pt(2 1 1) surface and thus falls in the range of barriers of the dehydrogenation–hydrogenation steps. In contrast, the barriers of C–C bond scission on the pathways to 2MP and 3MP on the stepped surface are raised to about 100 kJ mol^{-1}. Combining all these results, one is able to rationalize why the product distribution becomes close to statistical on small defect-rich Pt particles.

Although our study already answers important mechanistic questions, we would like to comment on three further aspects, which are beyond the goals of the present work, but may affect the overall selectivity at certain experimental conditions. First, other intermediates of MCP ring-opening have previously been discussed. For example, αβγ-tri-adsorbed intermediates were suggested to be responsible for the statistical rapture of the C–C bonds [18]. Gault postulated an αγ-di-adsorbed species, which participates in the formation of a metallocyclobutane [5]. A similar mechanism was theoretically studied [62] in the context of olefin metathesis catalyzed by transition metal complexes. We expect this type of intermediates to play a secondary role, but we are currently exploring them and a corresponding alternative mechanism in a separate work. Second, the selectivity toward *n*Hx was suggested to increase at a phase boundary [63]. Third, a recent study also reported that the shape of the Pt nano particles may affect the product distribution of MCP ring-opening [12]. The current study focused on the change in product selectivity due to steps/edges exposed by the metal component of the catalyst. The role of phase boundaries and the particles' morphology warrant further exploration.

Acknowledgments

We thank Prof. J.A. Lercher for stimulating discussions. We thank D. Basaran and H.A. Aleksandrov for assistance during the early stage of this study. Z.J.Z. gratefully acknowledges financial support by the International Doctorate Program NanoCat within the Bavarian Network of Excellence, an associated member of the TUM Graduate School at Technische Universität München. This work was supported by Deutsche Forschungsgemeinschaft and

Fonds der Chemischen Industrie (Germany). We also acknowledge generous computing resources at Leibniz Rechenzentrum München.

Appendix A. Supplementary material

Detailed reaction energy landscapes for MCP ring opening over Pt(1 1 1), alternative routes for C–C scission over Pt(2 1 1), Cartesian coordinates of the most significant intermediates and transition states. Supplementary data associated with this article can be found, in the online version, at doi:10.1016/j.jcat.2011.09.021.

References

[1] R.C. Santana, P.T. Do, M. Santikunaporn, W.E. Alvarez, J.D. Taylor, E.L. Sughrue, D.E. Resasco, Fuel 85 (2006) 643.
[2] A. Stanislaus, B.H. Cooper, Catal. Rev. –Sci. Eng. 36 (1994) 75.
[3] J. Scherzer, A.J. Gruia, Hydrocracking Science and Technology, Marcel Dekker, New York, 1996.
[4] H. Du, C. Fairbridge, H. Yang, Z. Ring, Appl. Catal. A 294 (2005) 1.
[5] F.G. Gault, Adv. Catal. 30 (1981) 1.
[6] C.J. Hagedorn, M.J. Weiss, T.W. Kim, W.H. Weinberg, J. Am. Chem. Soc. 123 (2001) 929.
[7] P.T. Do, E. Alvarez, D.E. Resasco, J. Catal. 238 (2006) 477.
[8] D. Kalakkad, S.L. Anderson, A.D. Logan, J. Pena, E.J. Braunschweig, C.H.F. Peden, A.K. Datye, J. Phys. Chem. 97 (1993) 1437.
[9] P.B. Weisz, E.W. Swegler, Science 126 (1957) 31.
[10] F. Roessner, U. Roland, J. Mol. Catal. A 112 (1996) 401.
[11] N. Győrffy, I. Bakos, S. Szabó, L. Tóth, U. Wild, R. Schlögl, Z. Paál, J. Catal. 263 (2009) 372.
[12] S. Alayoglu, C. Aliaga, C. Sprung, G.A. Somorjai, Catal. Lett. 141 (2011) 914.
[13] P. Samoila, M. Boutzeloit, C. Especel, F. Epron, P. Marécot, Appl. Catal. A 369 (2009) 104.
[14] Z. Wang, A.E. Nelson, Catal. Lett. 123 (2008) 226.
[15] R.J. Chimentão, G.P. Valença, F. Medina, J. Pérez-Ramírez, Appl. Surf. Sci. 253 (2007) 5888.
[16] N. Győrffy, A. Wootsch, S. Szabó, I. Bakos, L. Tóth, Z. Paál, Top. Catal. 46 (2007) 57.
[17] G.B. McVicker, M. Daage, M.S. Touvelle, C.W. Hudson, D.P. Klein, W.C. Baird Jr., B.R. Cook, J.G. Chen, S. Hantzer, D.E.W. Vaughan, E.S. Ellis, O.C. Feeley, J. Catal. 210 (2002) 137.
[18] G. Maire, G. Plouidy, J.C. Prudhomme, F.G. Gault, J. Catal. 4 (1965) 556.
[19] F. Garin, S. Aeiyach, P. Legare, G. Maire, J. Catal. 77 (1982) 323.
[20] F. Zaera, D. Godbey, G.A. Somorjai, J. Catal. 101 (1986) 73.
[21] A. Sárkány, J. Chem. Soc. Faraday Trans. 1 85 (1989) 1523.
[22] G. Del Angel, B. Coq, R. Dutartre, F. Figueras, J. Catal. 87 (1984) 27.
[23] W. Juszczyk, Z. Karpinski, J. Pielaszek, Z. Paál, J. Catal. 143 (1993) 583.
[24] B. Coq, A. Bittar, R. Dutartre, F. Figueras, J. Catal. 128 (1991) 275.
[25] V. Pallassana, M. Neurock, J. Catal. 191 (2000) 301.
[26] M. Neurock, R.A. van Santen, J. Phys. Chem. B 104 (2000) 11127.
[27] G. Jones, J.G. Jakobsen, S.S. Shim, J. Kleis, M.P. Andersson, J. Rossmeisl, F. Abild-Pedersen, T. Bligaard, S. Helveg, B. Hinnemann, J.R. Rostrup-Nielsen, I. Chorkendorff, J. Sehested, J.K. Nørskov, J. Catal. 259 (2008) 147.
[28] J. Joubert, F. Delbecq, P. Sautet, E. Le Roux, M. Taoufik, C. Thieuleux, F. Blanc, C. Coperet, J. Thivolle-Cazat, J.-M. Basset, J. Am. Chem. Soc. 128 (2006) 9157.
[29] J. Greeley, M. Mavrikakis, J. Am. Chem. Soc. 126 (2004) 3910.
[30] G. Brizuela, S. Simonetti, E. Pronsato, A. Juan, Surf. Sci. 556 (2004) 11.
[31] S. Simonetti, P. Jasen, E. Gonzalez, A. Juan, G. Brizuela, Appl. Surf. Sci. 252 (2006) 7515.
[32] N.C. Comelli, M.B. López, E.A. Castro, J. Mol. Struct.: THEOCHEM 726 (2005) 197.
[33] C. Becker, F. Delbecq, J. Breitbach, G. Hamm, D. Franke, F. Jäger, K. Wandelt, J. Phys. Chem. B 108 (2004) 18960.
[34] E. Germán, I. López-Corral, A. Juan, G. Brizuela, J. Mol. Catal. A 290 (2008) 23.
[35] G. Brizuela, N. Castellani, J. Mol. Catal. A 139 (1999) 209.
[36] G. Kresse, J. Hafner, Phys. Rev. B 49 (1994) 14251.
[37] G. Kresse, J. Furthmüller, Comput. Mater. Sci. 6 (1996) 15.
[38] J.P. Perdew, Y. Wang, Phys. Rev. B 45 (1992) 13244.
[39] P.E. Blöchl, Phys. Rev. B 50 (1994) 17953.
[40] G. Kresse, D. Joubert, Phys. Rev. B 59 (1999) 1758.
[41] H.J. Monkhorst, J.D. Pack, Phys. Rev. B 13 (1976) 5188.
[42] M. Methfessel, A.T. Paxton, Phys. Rev. B 40 (1989) 3616.
[43] G. Henkelman, H. Jónsson, J. Chem. Phys. 111 (1999) 7010.
[44] G. Mills, H. Jónsson, G.K. Schenter, Surf. Sci. 324 (1995) 305.
[45] H. Jónsson, G. Mills, K.W. Jacobsen, in: B.J. Berne, G. Ciccotti, D.F. Coker (Eds.), Classical and Quantum Dynamics in Condensed Phase Simulations, World Scientific, Singapore, 1998, p. 385.
[46] R. Kramer, H. Zuegg, J. Catal. 85 (1984) 530.
[47] J.R. Anderson, B.G. Baker, Proc. Roy. Soc. (London) A271 (1963) 402.
[48] Z.-X. Chen, H.A. Aleksandrov, D. Basaran, N. Rösch, J. Phys. Chem. C 114 (2010) 17683.
[49] M.-L. Yang, Y.-A. Zhu, C. Fan, Z.-J. Sui, D. Chen, X.-G. Zhou, Phys. Chem. Chem. Phys. 13 (2011) 3257.
[50] Z.-J. Zhao, L.V. Moskaleva, H.A. Aleksandrov, D. Basaran, N. Rösch, J. Phys. Chem. C 114 (2010) 12190.
[51] A.P. Graham, A. Menzel, J.P. Toennies, J. Chem. Phys. 111 (1999) 1676.
[52] W. Reckien, B. Kirchner, F. Janetzko, T. Bredow, J. Phys. Chem. C 113 (2009) 10541.
[53] F. Zaera, J. Am. Chem. Soc. 111 (1989) 8744.
[54] L.V. Moskaleva, H.A. Aleksandrov, D. Basaran, Z.-J. Zhao, N. Rösch, J. Phys. Chem. C 113 (2009) 15373.
[55] J.W. Medlin, M.D. Allendorf, J. Phys. Chem. B 107 (2003) 217.
[56] L.V. Moskaleva, Z.-X. Chen, H.A. Aleksandrov, A.B. Mohammed, Q. Sun, N. Rösch, J. Phys. Chem. C 113 (2009) 2512.
[57] D.W. Blakely, G.A. Somorjai, J. Catal. 42 (1976) 181.
[58] L. Guczi, J. Sárkány, J. Catal. 68 (1981) 190.
[59] A.T. Anghel, D.J. Wales, S.J. Jenkins, D.A. King, J. Chem. Phys. 126 (2007) 044710.
[60] I.V. Yudanov, A.V. Matveev, K.M. Neyman, N. Rösch, J. Am. Chem. Soc. 130 (2008) 9342.
[61] S. Schauermann, J. Hoffmann, V. Johánek, J. Hartmann, J. Libuda, H.-J. Freund, Angew. Chem. Int. Ed. 41 (2002) 2532.
[62] F.U. Axe, J.W. Andzelm, J. Am. Chem. Soc. 121 (1999) 5396.
[63] R. Kramer, H. Zuegg, J. Catal. 80 (1983) 446.